

ABSTRACT

We study compressed sensing when the sampling vectors are chosen from the rows of a unitary matrix. In the literature, these sampling vectors are typically chosen randomly; the use of randomness has enabled major empirical and theoretical advances in the field. However, in practice there are often certain crucial sampling vectors, in which case practitioners will depart from the theory and sample such rows deterministically. In this work, we derive an optimized sampling scheme for Bernoulli selectors which naturally combines random and deterministic selection of rows, thus rigorously deciding which rows should be sampled deterministically. This sampling scheme provides measurable improvements in image compressed sensing for both generative and sparse priors when compared to with-replacement and without-replacement sampling schemes, as we show with theoretical results and numerical experiments. Additionally, our theoretical guarantees feature improved sample complexity bounds compared to previous works, and novel denoising guarantees in this setting.

Keywords Compressed sensing; Bernoulli sampling; Optimal sampling; Denoising; Generative models.

PARTIALLY DETERMINISTIC SAMPLING FOR COMPRESSED SENSING WITH DENOISING GUARANTEES

A PREPRINT

Yaniv Plan*

Matthew S. Scott*

Ozgur Yilmaz*[†]

April 7, 2026

1 Introduction

Compressed sensing (CS) enables the recovery of high-dimensional signals with low-dimensional structure from far fewer measurements than their ambient dimension, a paradigm that led to “compressive signal acquisition” and has transformed fields like medical and seismic imaging, computational photography, and radar and remote sensing. Consider a signal $\mathbf{x}_0 \in \mathbb{K}^n$ (where \mathbb{K} is either \mathbb{R} or \mathbb{C}) that lies in or near a prior set $\mathcal{Q} \subseteq \mathbb{K}^n$ with effective dimensionality much smaller than n . We aim to reconstruct \mathbf{x}_0 from noisy measurements of the form $\mathbf{y} = A\mathbf{x}_0 + \boldsymbol{\epsilon}$, where $A \in \mathbb{K}^{m \times n}$ is a CS matrix with $m \ll n$, and $\boldsymbol{\epsilon} \sim \mathcal{N}(0, \sigma^2 I)$ represents Gaussian noise. We consider subsampled unitary CS matrices, which are of the form $A = SF$ for $F \in \mathbb{K}^{n \times n}$ a unitary matrix (e.g., Fourier), and $S \in \mathbb{R}^{m \times n}$ a random *sampling matrix*, a matrix each row of which has exactly one entry that is non-zero and identical. We call the rows of F *measurement vectors*. The sampling matrix S specifies a selection (and a uniform scaling) of these measurement vectors, and each selected measurement vector performs a noisy measurement on the true signal \mathbf{x}_0 via a noisy inner product.

This model matches applications like magnetic resonance imaging (MRI), where measurements are constrained to the Fourier domain [Lustig et al.(2007)Lustig, Donoho, and Pauly, Chauffert et al.(2014)Chauffert, Ciuciu, Kahn, and Weiss]. Early CS research recognized that not all measurements are equally informative; for example, low-frequency Fourier components are critical for natural images. This insight led to the development of *optimized sampling schemes*, also known in the literature as *optimal* or *near-optimal* sampling schemes, where measurements are prioritized based on their local coherences. (Local coherences quantify the alignment of each measurement vector with the prior set

*Department of Mathematics, University of British Columbia, Vancouver, BC, Canada.

[†]CNRS – PIMS International Research Laboratory

Author roles: Authors listed in alphabetic order. MS is the lead author of this manuscript.

Q [Candes and Romberg(2007), Puy et al.(2011)Puy, Vandergheynst, and Wiaux, Krahmer and Ward(2014)]. Optimized sampling schemes fall into the broader category of *variable-density sampling schemes*, which are randomized sampling schemes parameterized by probability vectors.

The simplest class of sampling distributions is with-replacement sampling, where measurement vectors are repeatedly drawn independently at random according to some fixed probability vector. Under this scheme, even the measurement vectors with the highest sampling probabilities can still be entirely missed, a phenomenon that can be significant in certain edge-case settings, as we show in a toy example in Section 6.

In an effort to address this limitation, Puy, Vandergheynst and Wiaux [Puy et al.(2011)Puy, Vandergheynst, and Wiaux] considered variable-density sampling with Bernoulli selectors, where each measurement vector is included according to its own independent Bernoulli random variable. For this type of sampling distribution, it is possible to set the probability weight of certain measurement vectors to 1, thereby including them deterministically. Bernoulli sampling schemes therefore naturally incorporate deterministic measurements into random sampling schemes. Block sampling emerged as another solution, where measurement vectors are arranged into blocks, and different blocks have their own sampling distributions [Bigot et al.(2016)Bigot, Boyer, and Weiss, Polak et al.(2015)Polak, Duarte, and Goeckel]. This paradigm allows for blocks of deterministically sampled measurements to be incorporated in a structured fashion.

Beyond the risk of entirely missing crucial measurements, with-replacement sampling has a second drawback: it allows for the repeated sampling of some measurement vectors, which yield no additional information about the true signal beyond their limited denoising effect. Both Bernoulli and without-replacement sampling are means of avoiding redundant selections [Hoppe et al.(2023)Hoppe, Krahmer, Verdun, Menzel, and Rauhut]. However, without-replacement schemes still cannot guarantee the inclusion of high-coherence measurement vectors, which may be missed with non-negligible probability in certain regimes. Optimized Bernoulli sampling stands out as a powerful solution, avoiding both redundant rows and missed critical measurements, while still allowing the sampling distribution to adapt to the local coherences. This hybrid approach is particularly advantageous in settings like MRI, where some low-frequency measurements are known to be essential, and their inclusion should therefore not be left up to chance. Moreover, Bernoulli sampling is widely adopted in CS literature due to its simplicity and compatibility with theoretical analysis (e.g., [Rudelson and Vershynin(2008)]).

In this paper, we advance the theory and practice of optimized Bernoulli sampling in a number of ways.

- **Denoising guarantees.** We establish the first denoising bounds for Bernoulli sampling under Gaussian noise and variable probability weights, extending the with-replacement theory of [Plan et al.(2025)Plan, Scott, Sheng, and Yilmaz] to this setting.
- **Closed-form probability weights.** We give a fully explicit expression for the optimized Bernoulli probability weights (Theorem 2.4), avoiding the need to solve an auxiliary equation for a normalizing constant as in [Adcock et al.(2024)Adcock, Cardenas, and Dexter] or an optimization problem as in [Puy et al.(2011)Puy, Vandergheynst, and Wiaux]. The closed-form expression simplifies implementation and makes the dependence on the local coherences and the number of measurements transparent.
- **Improved sample-complexity bounds.** Our bounds improve on those of optimized with-replacement sampling [Plan et al.(2025)Plan, Scott, Sheng, and Yilmaz] by replacing $\|\alpha\|_2$ with $L(\alpha, m)$ in the sample complexity and noise bound (see Theorem 2.1 and Theorem 2.4 for the definitions of α and L respectively). We show that $L(\alpha, m) \leq \|\alpha\|_2$; the enhancement comes from removing the dependence of the sample complexity on the local coherences of saturated measurements. When the number of measurements m is large, we demonstrate in Figure 1 that the improvement in the bound can be empirically significant in realistic settings.
- **General recovery guarantees for arbitrary Bernoulli weights.** We provide a recovery and denoising theory for any Bernoulli selector sampling scheme, with the optimized scheme obtained as the minimizer of the associated complexity bound.

Motivation for Bernoulli selectors. Bernoulli sampling schemes occupy a useful middle ground: they allow crucial rows to be included deterministically when their probability weights equal 1, while still enabling flexible randomization for the remaining measurements. This flexibility makes Bernoulli selectors especially attractive in applications such as MRI, where certain low-frequency measurements are indispensable and should not be left to chance.

Structure and flow. Section 2 presents our main recovery guarantee, Theorem 2.8, together with the optimized Bernoulli weights w° and the associated quantity $L(\alpha, m)$ that appears in the sample-complexity bound. The theoretical framework leading to this result is developed in the subsequent sections. This ordering is intentional: it allows the optimized sampling scheme and its consequences to be seen upfront, while the subsequent sections gradually build the theoretical framework that justifies it. With this in mind, the rest of the paper is organized as follows: Section 3

develops a general RIP-based recovery theory for an arbitrary sampling matrix: it introduces the truncation operator, establishes a signal recovery bound under an RIP assumption (Theorem 3.4), and derives general upper bounds on the noise term $\|\tilde{D}T(SD\alpha)\|_2$ (Theorem 3.5). In Section 4, we specialize this framework to Bernoulli selectors by introducing the tight Bernoulli complexity $\gamma(\alpha, w)$, proving an RIP bound for Bernoulli sampling (theorem 4.2), and combining it with the results of Section 3 to obtain the general recovery and denoising guarantees (Theorem 4.3) for arbitrary Bernoulli weights w . Section 5 then introduces a simplified upper bound on the Bernoulli complexity, shows that w° uniquely minimizes it, and identifies $L(\alpha, m)$ as the resulting optimized complexity value; it also contributes to the derivation of the bounds on the noise error term required for the main theorem. A toy example illustrating the behaviour of the optimized scheme is given in Section 6, and numerical comparisons with alternative sampling strategies appear in Section 7. The proofs of the results stated in these sections are collected in Section 8.

Much of the exposition follows an analogous structure to that of [Plan et al.(2025)Plan, Scott, Sheng, and Yilmaz], and readers familiar with that work may find the associated commentary helpful in interpreting the results developed here.

Notation. \mathbb{S}^{n-1} is the unit sphere in \mathbb{R}^n or \mathbb{C}^n depending on context. The simplex Δ^{n-1} is defined as:

$$\Delta^{n-1} = \left\{ \mathbf{p} \in \mathbb{R}^n \mid p_i \geq 0, \sum p_i = 1 \right\}.$$

We let B_2 be the ℓ_2 ball, and B_2^n be the ℓ_2 ball of dimension n specifically. We say that a set \mathcal{T} in a real or complex vector space is a *cone* when $\forall \lambda \in (0, \infty), \lambda\mathcal{T} = \mathcal{T}$, where $\lambda\mathcal{T} := \{\lambda t \mid t \in \mathcal{T}\}$. The self-difference $\mathcal{V} - \mathcal{V}$ is $\{\mathbf{v}_1 - \mathbf{v}_2 \mid \mathbf{v}_1, \mathbf{v}_2 \in \mathcal{V}\}$.

Let \mathbb{R}_+ be the non-negative real numbers, \mathbb{R}_{++} the strictly positive real numbers, and \mathbb{N} the natural numbers starting at 1. For a function f , we denote its range by $\text{range}(f)$, and its restriction to a subset C of its domain by $f|_C$. If f is a vector and C a subset of its support, then $f|_C$ is the $|C|$ -dimensional vector that is the restriction of f to C . Throughout this paper, we fix the field \mathbb{K} to be either \mathbb{C} or \mathbb{R} .

For a vector \mathbf{u} , its components are indexed as u_i . We denote by $\{\mathbf{e}_i\}_{i \in [n]}$ the canonical basis of \mathbb{R}^n . For $\ell \in \mathbb{N}$, the set $[\ell]$ comprises the integers from 1 to ℓ . We denote by $\text{supp } \mathbf{v}$ the support of \mathbf{v} , and by \mathbf{v}^2 the entry-wise square of \mathbf{v} . We say that a vector is *increasing* when $i \geq j \implies v_i \geq v_j$ and *decreasing* when $i \geq j \implies v_i \leq v_j$.

For an $m \times n$ matrix A , we denote its adjoint (the conjugate transpose) by A^* , its entries by $A_{i,j}$, and we denote by \mathbf{a}_i the conjugate transpose of its rows, i.e., $A = \sum_{i=1}^m \mathbf{e}_i \mathbf{a}_i^*$. The Euclidean norm of a vector $\mathbf{u} \in \mathbb{K}^n$ is $\|\mathbf{u}\|_2 := \sqrt{\mathbf{u}^* \mathbf{u}}$. The operator norm of a matrix A is $\|A\| := \sup_{\mathbf{u} \in B_2^n} \|A\mathbf{u}\|_2$. For matrices, given a vector $\mathbf{d} \in \mathbb{R}^n$, we denote by $\text{Diag}(\mathbf{d})$ the $n \times n$ diagonal matrix with diagonal entries \mathbf{d} . The identity matrix in \mathbb{R}^m is labeled I_m . Projection onto a closed set $\mathcal{T} \subseteq \mathbb{R}^n$ is denoted by $\Pi_{\mathcal{T}}$, mapping a vector \mathbf{x} to the element in \mathcal{T} that minimizes the Euclidean distance, with ties broken by choosing the lexicographically first (meaning that vectors are ordered by their first entry, then second, then third, and so on).

We use $\langle \cdot, \cdot \rangle$ to denote the inner product in \mathbb{K}^n ; specifically, the canonical inner product when \mathbb{K} is \mathbb{R} , and the complex inner product $\langle \mathbf{u}, \mathbf{v} \rangle = \mathbf{u}^* \mathbf{v}$ when \mathbb{K} is \mathbb{C} . We also denote by $\mathcal{R}\langle \cdot, \cdot \rangle$ the real part of the inner product (which is just the canonical inner product when \mathbb{K} is \mathbb{R}).

We employ the notation $a \lesssim b$ if $a \leq Cb$ where C is an absolute constant, potentially different for each instance. We denote $X \sim \mathcal{N}(\mu, \sigma^2)$ to be the Gaussian random variable with mean μ and variance σ^2 . A random Gaussian vector $g \sim \mathcal{N}(0, I_m)$ is a random vector in \mathbb{R}^m which has i.i.d. $\mathcal{N}(0, 1)$ Gaussian entries. A complex random Gaussian vector $g \sim \mathcal{N}(0, I_m)$, $g \in \mathbb{C}^m$, is a random vector in \mathbb{C}^m with entries that have real and imaginary parts individually $\stackrel{\text{iid}}{\sim} \mathcal{N}(0, 1)$.

2 Main result

To set up our main result, we introduce a number of mathematical objects. We begin with the *local coherence* which quantifies the alignment of a measurement vector with a cone.

Definition 2.1 (Local coherence). The *local coherence* of a vector $\phi \in \mathbb{K}^n$ with respect to a cone $\mathcal{T} \subseteq \mathbb{R}^n$ is defined as

$$\alpha_{\mathcal{T}}(\phi) := \sup_{\mathbf{x} \in \mathcal{T} \cap B_2} |\phi^* \mathbf{x}|.$$

The *local coherences* of a unitary matrix $F \in \mathbb{K}^{n \times n}$ with respect to a cone $\mathcal{T} \subseteq \mathbb{K}^n$ is defined as the vector $\alpha \in \mathbb{R}_+^n$ with entries $\alpha_j := \alpha_{\mathcal{T}}(\mathbf{f}_j)$, where \mathbf{f}_j is the conjugate transpose of the j^{th} row of F .

We note that the local coherence vector can be hard to compute depending on the structure of \mathcal{T} . We give two methods to heuristically approximate it in Section 7.

Recall that we consider CS matrices of the form SF , where F is a $n \times n$ unitary matrix (for example, F can be the Fourier matrix), and S is a *sampling matrix* with Bernoulli selectors, which we now define.

Definition 2.2 (Bernoulli selector sampling matrix). Let $\mathbf{w} \in [0, 1]^n \cap m\Delta^{n-1}$ be a *probability weight vector* and $A \in \mathbb{R}^{n \times n}$ be a random diagonal matrix with entries $A_{i,i} = \sqrt{\frac{n}{m}}\xi_i$, where $\xi_i \stackrel{\text{iid}}{\sim} \text{Ber}(w_i)$. We define the *Bernoulli sampling matrix* to be the $\tilde{m} \times n$ matrix S obtained by removing the rows of A that are 0.

Note that a Bernoulli sampling matrix has a random number of rows \tilde{m} satisfying $\mathbb{E}\tilde{m} = m$. We outline the problem of robust signal recovery in greater detail.

Setup 2.3 ([Plan et al.(2025)Plan, Scott, Sheng, and Yilmaz, Setup 2.5]). **Prior and true signal**

Let $\mathbf{x}_0 \in \mathbb{R}^n$ be a signal, and $\mathcal{Q} \subseteq \mathbb{R}^n$ be a prior set such that $\mathcal{Q} - \mathcal{Q} \subseteq \mathcal{T}$, for $\mathcal{T} \subseteq \mathbb{R}^n$ a union of M subspaces each of dimension at most ℓ . We think of \mathbf{x}_0 as being close to \mathcal{Q} ; $\mathbf{x}^\perp := \mathbf{x}_0 - \Pi_{\mathcal{Q}}\mathbf{x}_0$ quantifies the model mismatch.

Measurement acquisition

Let $F \in \mathbb{K}^{n \times n}$ be a unitary matrix. Suppose that $\boldsymbol{\alpha}$ is the vector of local coherences of F with respect to \mathcal{T} . Let S be a possibly random *sampling matrix*, and define the measurements

$$\mathbf{b} = SF\mathbf{x}_0 + \boldsymbol{\eta},$$

where the noise is $\boldsymbol{\eta} = \frac{\sigma\mathbf{g}}{\sqrt{m}}$ with $\mathbf{g} \sim \mathcal{N}(0, I_m)$ being a Gaussian vector in \mathbb{K}^m . Here, $\mathbb{E}[\|\boldsymbol{\eta}\|_2^2]$ is σ^2 when \mathbb{K} is \mathbb{R} and $2\sigma^2$ when \mathbb{K} is \mathbb{C} . Thus, σ determines the size of the noise. With this normalization, $\frac{1}{\sigma}$ can be thought of as the Signal-to-Noise Ratio (SNR) up to an absolute constant.

Signal reconstruction

Knowing only \mathbf{b}, S and F , we (approximately) recover the true signal \mathbf{x}_0 by (approximately) solving the following optimization problem:

$$\underset{\mathbf{x} \in \mathcal{Q}}{\text{minimize}} \|\tilde{D}SF\mathbf{x} - \tilde{D}\mathbf{b}\|_2^2 \quad (2.1)$$

where $\tilde{D} := \sqrt{\frac{m}{n}}\text{Diag}(S\mathbf{d})$ is a diagonal preconditioning matrix for some $\mathbf{d} \in \mathbb{R}^n$. Note that in terms of $D := \text{Diag}(\mathbf{d})$, the preconditioned CS matrix $\tilde{D}SF$ can be written as SDF . This demonstrates that the preconditioning is, in fact, an element-wise scaling operation applied to individual rows of F . The use of the preconditioner \tilde{D} is prevalent in the literature (e.g., see [Krahmer and Ward(2014)]), and seems to be necessary to obtain the RIP (see Theorem 3.3 in Section 3) on the CS matrix when the sampling probabilities are non-uniform. Intuitively, it is chosen so as to “balance out” the effect of the sampling probabilities on the expected size of the measurement vectors. We approximately solve the optimization problem Equation (2.1) and obtain an $\hat{\mathbf{x}} \in \mathcal{Q}$ such that

$$\|\tilde{D}SF\hat{\mathbf{x}} - \tilde{D}\mathbf{b}\|_2^2 \leq \min_{\mathbf{x} \in \mathcal{Q}} \|\tilde{D}SF\mathbf{x} - \tilde{D}\mathbf{b}\|_2^2 + \varepsilon \quad (2.2)$$

for some small optimization error $\varepsilon > 0$.

Given the above setup, our objective is to bound the error $\|\mathbf{x}_0 - \hat{\mathbf{x}}\|_2$ in terms of the noise level σ , the optimization error ε , and the distance of the true signal \mathbf{x}_0 to the prior \mathcal{Q} ($\|\mathbf{x}^\perp\|$, the approximation error).

Our setting is identical to [Plan et al.(2025)Plan, Scott, Sheng, and Yilmaz, Setup 2.5], with the only difference that we let S be a sampling matrix with Bernoulli selectors. As will be made apparent, the theoretical challenge (and associated benefit) of Bernoulli selector sampling lies in the possibility of measurement vectors being sampled with probability 1. We call such measurement vectors *saturated*.

We specify the *optimized* sampling scheme for Bernoulli selectors. Recall that in this work, a vector $\boldsymbol{\alpha}$ is “increasing” when $i \leq j \implies \alpha_i \leq \alpha_j$.

Definition 2.4 (Optimized Bernoulli weights). Let $m < n$ and $\boldsymbol{\alpha} \in \mathbb{R}_{++}^n$ be a local coherence vector which, without loss of generality, we assume has increasing entries (otherwise, re-index the vector $\boldsymbol{\alpha}$). Let

$$R^2(j; \boldsymbol{\alpha}, m) = \frac{m\|\boldsymbol{\alpha}_{[j]}\|_2^2}{j - (n - m)},$$

and

$$J = \max \left\{ j \in [n] : \frac{m\alpha_j^2}{R^2(j; \boldsymbol{\alpha}, m)} < 1 \right\}. \quad (2.3)$$

Then for $L^2(\boldsymbol{\alpha}, m) := R^2(J; \boldsymbol{\alpha}, m)$, the optimized probability weights are

$$w_j^\circ = \min \left(\frac{m\alpha_j^2}{L^2(\boldsymbol{\alpha}, m)}, 1 \right).$$

The optimized sampling vector is chosen so as to guarantee a small sample complexity in Theorem 2.8.

Remark 2.5. Theorem 2.4 assumes that the entries of $\boldsymbol{\alpha}$ are ordered increasingly; for any local coherence vector that is not already ordered, we evaluate $L(\boldsymbol{\alpha}, m)$ by first re-ordering $\boldsymbol{\alpha}$ increasingly and then applying the same definition.

Remark 2.6. The quantity $L(\boldsymbol{\alpha}, m)$ from Definition 2.4 will later be identified (in Section 5) as the optimized sample-complexity factor obtained by minimizing a simplified Bernoulli complexity measure $\eta(\boldsymbol{\alpha}, \boldsymbol{w})$ over all feasible Bernoulli probability weights with the explicit weights \boldsymbol{w}° from Definition 2.4 arising as the (unique) minimizer.

Proposition 2.7 (Norm of the optimized probability weights). *In Theorem 2.4,*

1. J is the number of unsaturated measurement vectors.
2. $\sum_{i=1}^n w_i^\circ = m$, that is, in expectation m rows are sampled.

We defer the proof of Theorem 2.7 to Section 8.5. We are now ready to state our main recovery guarantee for optimized Bernoulli sampling.

Theorem 2.8 (Optimized Bernoulli CS on union of subspaces). *Under Theorem 2.3, for some $\delta > 0$, with $L^2(\boldsymbol{\alpha}, m)$ as in Theorem 2.4, suppose that*

$$m \gtrsim L^2(\boldsymbol{\alpha}, m) \left(\log \ell + \log M + \log \frac{20}{\delta} \right). \quad (2.4)$$

With the sampling matrix S governed by the optimized probability weights \boldsymbol{w}° , and $D = \text{diag}(\mathbf{d})$ where $d_i = \sqrt{\frac{m}{nw_i^\circ}}$, the following holds with probability at least $1 - \delta$.

For any $\mathbf{x}_0 \in \mathbb{R}^n$, with $\varepsilon, \hat{\mathbf{x}}, \mathbf{x}^\perp$ as in Theorem 2.3, we have that

$$\begin{aligned} \|\hat{\mathbf{x}} - \mathbf{x}_0\|_2 \leq 9 \frac{\sigma}{\sqrt{m}} L(\boldsymbol{\alpha}, m) \sqrt{\min \left(\frac{5}{4\delta} + \frac{m}{nL^2(\boldsymbol{\alpha}, m)}, \frac{1}{n \min(\boldsymbol{\alpha})^2} \right)} \left(\sqrt{\ell} + \sqrt{\log M} + \sqrt{\log \frac{20}{\delta}} \right) \\ + \|\mathbf{x}^\perp\| + 6 \|SDF\mathbf{x}^\perp\|_2 + \frac{3}{2} \sqrt{\varepsilon}. \end{aligned}$$

The proof of Theorem 2.8 will follow from results in the following sections.

Remark 2.9. Theorem 2.8 implies the following. Let $m \gtrsim L^2(\boldsymbol{\alpha}, m) (\log \ell + \log M + 1)$, $\mathbf{x}_0 \in \mathcal{Q}$. We also require, with $\boldsymbol{\alpha}$ re-indexed so that it is increasing, that $\|\boldsymbol{\alpha}_{|\leq n-m+1}\|_2^2 \gtrsim \frac{m}{n}$, which is a mild technical condition on the local coherences (see Theorem 2.12). Then with probability at least 0.99, any exact minimizer $\hat{\mathbf{x}}$ of Equation (2.1) is such that

$$\|\hat{\mathbf{x}} - \mathbf{x}_0\|_2 \lesssim \frac{\sigma}{\sqrt{m}} L(\boldsymbol{\alpha}, m) \left(\sqrt{\ell} + \sqrt{\log M} + 1 \right).$$

The sample complexity in Theorem 2.8 is unconventional in its dependence of the function L on m , on the r.h.s. of Equation (2.4). We leave it in this form because we do not see a way to isolate the explicit bound on m . Nonetheless, our bound provides meaningful intuition and improves over the analogous bound for with-replacement sampling.

Proposition 2.10 (Upper bound Bernoulli L with local coherences). *Given an increasing vector $\boldsymbol{\alpha} \in \mathbb{R}_{++}^n$ and $m \in \mathbb{N}$, let $L(\boldsymbol{\alpha}, m)$ be as in Theorem 2.4 (equivalently, Theorem 5.2). Then*

$$\|\boldsymbol{\alpha}_{|\leq n-m+1}\|_2 \leq L(\boldsymbol{\alpha}, m) \leq \|\boldsymbol{\alpha}\|_2.$$

The quantity $\|\boldsymbol{\alpha}\|_2$ is found in place of $L(\boldsymbol{\alpha}, m)$ in [Plan et al.(2025)Plan, Scott, Sheng, and Yilmaz, Theorem 2.1] for an analogous optimized with-replacement sampling scheme. Our sample complexity bound for Bernoulli sampling therefore improves on the with-replacement analogue.

Proposition 2.11 (Monotonicity of L in m). *The function $L(\boldsymbol{\alpha}, m)$ is decreasing in m .*

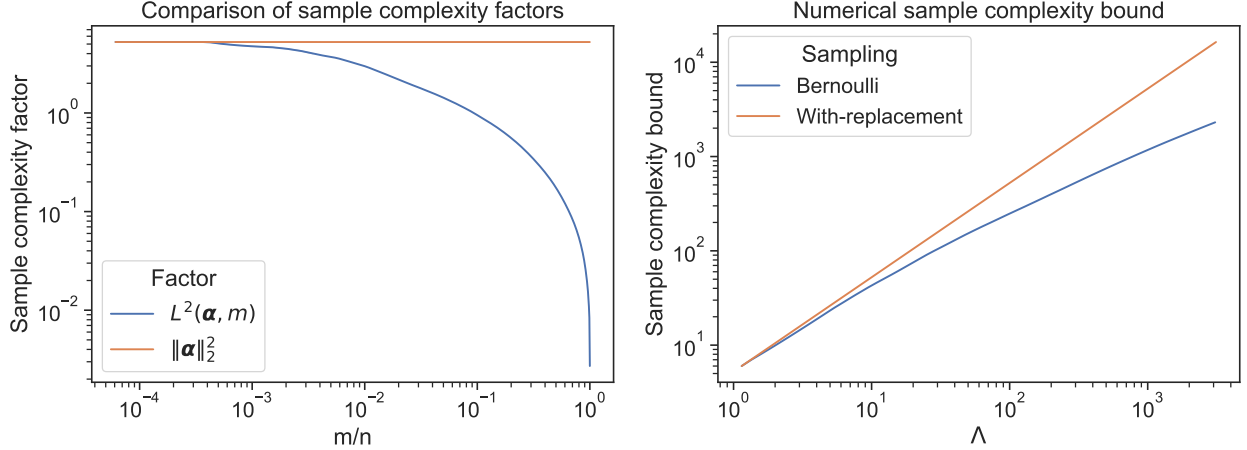


Figure 1: We consider a fixed coherence vector α across all experiments, which is the local coherences of the DFT matrix on the flower dataset [Nilsback and Zisserman(2008)] as prior set ($n = 16384$). The right plot compares numerically the bound on m induced by a bound of the form $m \geq L^2(\alpha, m)\Lambda$ (see the above discussion).

We defer the proof of Theorem 2.10 and the proof of Theorem 2.11 to Section 8.5.

Theorem 2.11 suggests that the improvement in the sample complexity bound becomes significant for large values of m . This makes sense intuitively because the quantity $L^2(\alpha, m)$ is the sum of squared local coherences, but limited to unsaturated entries only (which have smaller local coherences), and then suitably re-normalized. As m grows, more entries become saturated, and the associated local coherences (which are the larger local coherences) are excluded from the computation of $L^2(\alpha, m)$. So when m becomes large enough to “eat up” large local coherences, the implicit sample complexity bound on m in Theorem 2.8 will be easily be satisfied, because the value of $L^2(\alpha, m)$ will drop. We compute numerically the extent of this drop in Figure 1.

To compute the explicit bound, recall that our sample complexity bound is of the form $m \geq L^2(\alpha, m)\Lambda$ for some quantity $\Lambda \in \mathbb{R}_+$. In Theorem 2.8, we have this type of bound with $\Lambda = (\log \ell + \log M + \log \frac{20}{\delta})$. We derive an associated explicit bound on m : with $\Phi(m) := \frac{m}{L^2(\alpha, m)}$, we have $m \geq \Phi^{-1}(\Lambda)$. The inverse is well-defined because $L(\alpha, m)$ is decreasing in m by Theorem 2.11, and therefore $\Phi : \mathbb{R} \rightarrow \mathbb{R}$ is a strictly increasing function, making Φ invertible when restricting its codomain to match its range. We compute the values of the explicit sample complexity bound for a realistic coherence vector in Figure 1, comparing it with the analogous bound in the with-replacement setting.

Remark 2.12. The term $\frac{1}{12} \frac{m}{nL^2}$ in Theorem 2.8 is usually small. Indeed, from Theorem 2.10 it follows that after re-ordering α to be increasing, $\frac{m}{nL^2} \leq \frac{m}{n} \frac{1}{\|\alpha_{|\leq n-m+1}\|_2^2}$. This term becomes significant only when

$$\|\alpha_{|\leq n-m+1}\|_2^2 \lesssim \frac{m}{n}.$$

All but the top m local coherences would have to be on the order of $\frac{\sqrt{m}}{n}$ (assuming that $m \ll n$). The expected coherence of a randomly rotated vector with a k -dimensional subspace is about $\sqrt{\frac{k}{n}}$, so the typical size of the truncated local coherence vector is on the order of k . Therefore, for the additional term to be significant, the local coherences would have to be atypically small.

3 General signal recovery

In this section we develop a general recovery framework that applies to any sensing matrix satisfying a suitable RIP condition. Working in the setting of Theorem 2.3, we derive a signal recovery guarantee under RIP assumptions on the preconditioned CS matrix SDF . This abstract result forms the backbone of our analysis: Section 4 will verify the required RIP condition specifically for Bernoulli selectors, and define the complexity quantity $\gamma(\alpha, w)$ under which these bounds hold.

To control the noise term appearing in our recovery bound, we introduce a simple truncation operator that limits the magnitude of a vector to unit scale by truncating its support to sufficiently many entries (using the coordinate order).

Definition 3.1 (Unit truncation). Given some $\mathbf{v} \in \mathbb{R}^n$, let

$$I = \min \{ \bar{I} \in [n] \mid \|\mathbf{v}|_{[\bar{I}]}\|_2 \geq 1 \}.$$

Then define the unit truncation operator $\mathbb{T} : \mathbb{K}^n \rightarrow \mathbb{K}^n$ to have entries

$$\mathbb{T}(\mathbf{v})_i := \begin{cases} v_i & i < I, \\ \sqrt{1 - \|\mathbf{v}|_{[I-1]}\|_2^2} & i = I, \\ 0 & i > I. \end{cases}$$

Remark 3.2. The truncation operator is used solely to bound the contribution of the noise term in our analysis; it does not affect the structure of the recovery argument.

Next we recall the general version of the celebrated *restricted isometry property* (RIP).

Definition 3.3 (Restricted Isometry Property). Let $\mathcal{T} \subseteq \mathbb{R}^n$ be a cone and $A \in \mathbb{K}^{m \times n}$ a matrix. We say that A satisfies the *Restricted Isometry Property* (RIP) when

$$\sup_{u \in \mathcal{T} \cap \mathcal{S}^{n-1}} \left| \|Au\|_2 - 1 \right| \leq \frac{1}{3}.$$

The following lemma provides a general signal recovery guarantee under an RIP assumption. It was originally stated in [Plan et al.(2025)Plan, Scott, Sheng, and Yilmaz, Theorem 3.3], we restate it here for completeness.

Lemma 3.4 (Signal recovery with the RIP; [Plan et al.(2025)Plan, Scott, Sheng, and Yilmaz, Theorem 3.3]). *Under Theorem 2.3, let S be some fixed sampling matrix and suppose that SDF satisfies the RIP on \mathcal{T} . Then for $t > 0$, the following holds with probability at least $1 - 2 \exp(-t^2)$.*

For any $\mathbf{x}_0 \in \mathbb{R}^n$, with $\varepsilon, \hat{\mathbf{x}}, \mathbf{x}^\perp$ as in Theorem 2.3, we have that

$$\begin{aligned} \|\hat{\mathbf{x}} - \mathbf{x}_0\|_2 &\leq 9 \frac{\sigma}{\sqrt{m}} \|\tilde{D}\mathbb{T}(SD\boldsymbol{\alpha})\|_2 \left(\sqrt{\ell} + \sqrt{\log M} + t \right) \\ &\quad + \|\mathbf{x}^\perp\| + 6\|SDF\mathbf{x}^\perp\|_2 + \frac{3}{2}\sqrt{\varepsilon}. \end{aligned}$$

To apply the recovery bound of Theorem 3.4, we require estimates on the noise factor $\|\tilde{D}\mathbb{T}(SD\boldsymbol{\alpha})\|_2$. The next result gives general upper bounds for this term, which will later be specialized to the Bernoulli setting in Section 4.

Proposition 3.5 (Bounds on the noise error). *With any $\mathbf{d} \in \mathbb{R}_{++}^n$, $\boldsymbol{\alpha} \in \mathbb{R}_{++}^n$, and S a fixed $m \times n$ sampling matrix such that $S\mathbf{d}$ is decreasing, with $D = \text{Diag}(\mathbf{d})$ and $\tilde{D} = \text{Diag}(\sqrt{\frac{m}{n}}S\mathbf{d})$ we have that*

$$\|\tilde{D}\mathbb{T}(SD\boldsymbol{\alpha})\|_2 \leq \max(S\mathbf{d}) \leq \max(\mathbf{d}). \quad (3.1)$$

Furthermore, with

$$\begin{aligned} I &= |\text{supp } \mathbb{T}(SD\boldsymbol{\alpha})| \\ \|\tilde{D}\mathbb{T}(SD\boldsymbol{\alpha})\|_2 &\leq \|(SD^2\boldsymbol{\alpha})|_{[I]}\|_2 \leq \|SD^2\boldsymbol{\alpha}\|_2. \end{aligned} \quad (3.2)$$

Proof of Theorem 3.5. We write

$$\|\tilde{D}\mathbb{T}(SD\boldsymbol{\alpha})\|_2 = \sqrt{\sum_{i=1}^I (S\mathbf{d})_i^2 \mathbb{T}(SD\boldsymbol{\alpha})_i^2}.$$

Under the square root, we find a convex combination of the entries of $S\mathbf{d}$ with convex coefficients $\mathbb{T}(SD\boldsymbol{\alpha})_i^2$. The first bound in Equation (3.1) follows from bounding the convex combination by the size of the maximal element.

To see that Equation (3.2) holds, it suffices to check that $(SD\boldsymbol{\alpha})|_{[I]}$ dominates $\mathbb{T}(SD\boldsymbol{\alpha})$ entry-wise. \square

The recovery lemma and noise bounds established in this section do hold for arbitrary sampling matrices. In the next section, we specialize these results to the Bernoulli setting by introducing the complexity measure $\gamma(\boldsymbol{\alpha}, \mathbf{w})$ and establishing conditions under which a Bernoulli CS matrix has the RIP (with high probability), conditions under which Theorem 3.4 then applies.

4 Variable-density sampling

In this section we specialize the general recovery framework developed in Section 3 to the Bernoulli setting. Given a Bernoulli selector matrix S with weights \mathbf{w} , we introduce a tight Bernoulli complexity measure $\gamma(\boldsymbol{\alpha}, \mathbf{w})$ that captures the interaction between the sampling distribution and the local coherence vector. This quantity is fundamental in establishing RIP conditions for Bernoulli sampling, and serves as the bridge between the general recovery bound of Theorem 3.4 and the optimized sampling scheme developed in Section 5.

Definition 4.1 (Tight Bernoulli complexity). Let $\boldsymbol{\alpha} \in \mathbb{R}_{++}^n$ be a vector of local coherences and let $\mathbf{w} \in (0, 1]^n \cap m\Delta^{n-1}$ for $m < n$. We define

$$\gamma(\boldsymbol{\alpha}, \mathbf{w}) := \max_{j \in [n]} \alpha_j \sqrt{m} \max \left(\sqrt{\frac{1-w_j}{w_j}}, 1 \right) \mathbf{1}_{\{w_j < 1\}}.$$

The next result shows that the preconditioned sensing matrix $\tilde{D}SF$ (equivalently, SDF) satisfies the RIP under conditions controlled by the Bernoulli complexity $\gamma(\boldsymbol{\alpha}, \mathbf{w})$. This provides the main technical link between the sampling distribution \mathbf{w} and the RIP-based recovery bound of Theorem 3.4.

Lemma 4.2 (RIP of CS matrix on a union of subspaces). *Considering Theorem 2.3, let S be a sampling matrix with probability weights $\mathbf{w} \in m\Delta^{n-1} \cap (0, 1]$. Let $D = \text{Diag}(\mathbf{d})$ where $d_i = \sqrt{\frac{m}{nw_i}}$. For $t > 0$, and γ as defined in Theorem 4.1, suppose that*

$$m \gtrsim \gamma^2(\boldsymbol{\alpha}, \mathbf{w}) (\log \ell + \log M + t^2).$$

Then for S a sampling matrix with probability weights \mathbf{w} , SDF has the RIP on \mathcal{T} with probability at least $1 - 2\exp(-t^2)$.

The proof can be found in Section 8.1. Combining Theorem 4.2 with Theorem 3.4 yields the following compressed sensing recovery and denoising guarantees for variable-density sampling.

Theorem 4.3 (CS with Bernoulli and denoising on unions of subspaces). *Under Theorem 2.3, with γ the complexity function given by Theorem 5.1 and $\delta > 0$, suppose that*

$$m \gtrsim \gamma^2(\boldsymbol{\alpha}, \mathbf{w}) \left(\log \ell + \log M + \log \frac{4}{\delta} \right).$$

Sample the sampling matrix S with probability weights \mathbf{w} . Let $D = \text{Diag}(\mathbf{d})$ and $\tilde{D} = \sqrt{\frac{m}{n}} \text{Diag}(S\mathbf{d})$, where $d_i = \sqrt{\frac{m}{nw_i}}$. Then, the following holds with probability at least $1 - \delta$.

For any $\mathbf{x}_0 \in \mathbb{R}^n$, with $\hat{\mathbf{x}}, \mathbf{x}^\perp, \varepsilon$ as in Theorem 2.3, we have that

$$\begin{aligned} \|\hat{\mathbf{x}} - \mathbf{x}_0\|_2 &\leq 9 \frac{\sigma}{\sqrt{m}} \|\tilde{D}\mathbb{T}(SD\boldsymbol{\alpha})\|_2 \left(\sqrt{\ell} + \sqrt{\log M} + \sqrt{\log \frac{4}{\delta}} \right) \\ &\quad + \|\mathbf{x}^\perp\| + 6\|SDF\mathbf{x}^\perp\|_2 + \frac{3}{2}\sqrt{\varepsilon}. \end{aligned}$$

See the proof in Section 8.3.

Theorem 4.3 applies to any Bernoulli sampling distribution and expresses the recovery guarantee explicitly in terms of the complexity $\gamma(\boldsymbol{\alpha}, \mathbf{w})$. In the next section, we introduce a simplified complexity measure $\eta(\boldsymbol{\alpha}, \mathbf{w})$ and show that the optimized weights \mathbf{w}° minimize this quantity, thereby identifying the optimized complexity value $L(\boldsymbol{\alpha}, m)$ appearing in the main theorem.

5 Optimized sampling

Here, we define a simplified complexity $\eta(\boldsymbol{\alpha}, \mathbf{w})$, optimize it in closed form, and use the resulting weights to control the noise-sensitivity term.

Definition 5.1 (Simpler complexity function). Let $\boldsymbol{\alpha} \in \mathbb{R}_{++}^n$ be a vector of local coherences and $\mathbf{w} \in (0, 1]^n \cap m\Delta^{n-1}$ for $m < n$. We define

$$\eta(\boldsymbol{\alpha}, \mathbf{w}) := \max_{j \in [n]} \alpha_j \sqrt{\frac{m}{w_j}} \mathbf{1}_{\{w_j < 1\}}.$$

A direct comparison shows that $\gamma(\boldsymbol{\alpha}, \mathbf{w}) \leq \eta(\boldsymbol{\alpha}, \mathbf{w})$ for all feasible weights $\mathbf{w} \in (0, 1]^n \cap m\Delta_{n-1}$. In particular, any upper bound expressed in terms of $\eta(\boldsymbol{\alpha}, \mathbf{w})$ can be used to control the RIP condition from Lemma 4.2 via $\gamma(\boldsymbol{\alpha}, \mathbf{w})$. The vector of optimized probability weights is the minimizer of η over the feasible Bernoulli weights.

Proposition 5.2 (Optimize simple Bernoulli selector sampling). *For a fixed vector $\boldsymbol{\alpha} \in \mathbb{R}_{++}$ and the function η as in Theorem 5.1, let \mathbf{w}° be the optimized probability vector from Theorem 2.4. Then*

$$\min_{\mathbf{w} \in (0, 1]^n \cap m\Delta_{n-1}} \eta(\boldsymbol{\alpha}, \mathbf{w}) = \eta(\boldsymbol{\alpha}, \mathbf{w}^\circ) = L(\boldsymbol{\alpha}, m),$$

where \mathbf{w}° is the unique minimizer.

We defer the proof to Section 8.4.

For the optimized sampling scheme, there is a simple probabilistic upper-bound on the signal recovery noise error term.

Lemma 5.3 (Tail bound for the noise sensitivity under optimized Bernoulli sampling). *Let $\boldsymbol{\alpha} \in \mathbb{R}_{++}^n$ and $m \in \mathbb{N}$, and let \mathbf{w}° , J , and $L(\boldsymbol{\alpha}, m)$ be as in Theorem 2.4. Let $D = \text{Diag}(\mathbf{d})$ and $\tilde{D} = \text{Diag}(\sqrt{\frac{m}{n}}S\mathbf{d})$, where $d_i = \sqrt{\frac{m}{n\mathbf{w}_i^\circ}}$. Let S be the Bernoulli sampling matrix with probability weights \mathbf{w}° , with rows re-ordered so that $S\mathbf{d}$ is decreasing. Then for any $t > 0$,*

$$\|\tilde{D}\mathbb{T}(SD\boldsymbol{\alpha})\|_2 \leq L(\boldsymbol{\alpha}, m) \sqrt{\min\left(\frac{1}{t} + \frac{m}{nL^2(\boldsymbol{\alpha}, m)}, \frac{1}{n \min(\boldsymbol{\alpha})^2}\right)}$$

with probability at least $1 - t$, where \mathbb{T} is the unit truncation operator from Theorem 3.1.

This completes the last ingredient needed for the optimized recovery guarantee stated in Theorem 2.8. The proof follows by combining Theorem 4.3 with Theorem 5.3 via a union bound (see the proof in Section 8.3).

Next, we examine the difference between Bernoulli sampling and without-replacement sampling. In the latter, one repeatedly draws measurement vectors according to a fixed distribution (as in with-replacement sampling), but rejects any draw that repeats a previously selected vector, continuing until m distinct measurement vectors are obtained. Equivalently, this procedure can be viewed as sequential sampling without replacement in which, after each accepted draw, the distribution is renormalized over the remaining (unselected) vectors. For completeness, we prove this equivalence in Section A. Without-replacement sampling avoids the pitfall of with-replacement sampling, which often re-samples measurement vectors with diminishing returns. This drawback becomes pronounced for optimized sampling schemes, as we show in Section 7. Optimized without-replacement sampling with theoretical guarantees was introduced in [Hoppe et al.(2023)Hoppe, Kraemer, Verdun, Menzel, and Rauhut].

In the next section we outline a toy example consisting of a simple local coherence vector, for which we show that optimized Bernoulli sampling significantly outperforms optimized without-replacement in sampling complexity.

6 Toy example

Consider a prior set $\mathcal{Q} \subseteq \mathbb{R}^n$ to be the union of $\{e_1\}$ and of a subspace \mathcal{U} consisting of vectors supported on $\{2, \dots, n\}$, and which is maximally incoherent with the canonical basis.

We now define \mathcal{U} explicitly: let $A \in \mathbb{R}^{(n-1) \times (n-1)}$ be the discrete Fourier transform matrix in \mathbb{R}^{n-1} , and let $M \in \mathbb{R}^{n \times (n-1)}$ be the matrix A padded with zeros in its first row, in the sense that $M_{1,j} = 0$, and $M_{i,j} = A_{i-1,j}$ for $i \in \{2, \dots, n\}$ and $j \in [n-1]$. We define \mathcal{U} to be the span of the first $k-1$ columns of M .

Next, take the identity matrix I as the unitary measurement matrix F , so that the CS matrix SF reduces to S .

For this choice of \mathcal{Q} and F , one can check that S has the RIP if and only if the following hold:

1. The measurement vector e_1 is sampled,
2. Measurement vectors corresponding to at least $k-1$ distinct indices out of $\{2, \dots, n\}$ are sampled.

We show that in this simple setting, optimized without-replacement sampling fails to sample the first measurement vector with constant probability as $n \rightarrow \infty$, even for large k . In contrast, under the same setup, the probability of failure for the optimized Bernoulli selector sampling scheme vanishes.

Since \mathcal{U} is a fully-incoherent $(k-1)$ -dimensional subspace in the $(n-1)$ -dimensional subspace of vectors supported on $\{2, \dots, n\}$, it follows from [Berk et al.(2022)Berk, Brugiapaglia, Joshi, Plan, Scott, and Yilmaz, Proposition 3.1]

that the local coherence vector of I with respect to \mathcal{Q} is

$$\alpha = \left\{ 1, \sqrt{\frac{k-1}{n-1}}, \dots, \sqrt{\frac{k-1}{n-1}} \right\}.$$

Then the optimized probability vector defined in [Plan et al.(2025)Plan, Scott, Sheng, and Yilmaz, Definition 2.6] is

$$\mathbf{p}^* = \left\{ \frac{1}{k}, \frac{k-1}{k(n-1)}, \dots, \frac{k-1}{k(n-1)} \right\}.$$

Sampling sequentially without replacement according to \mathbf{p}^* , the probability that the first measurement vector fails to be sampled on the next draw after ℓ draws is

$$1 - \frac{1}{k} \frac{1}{1 - \ell \frac{k-1}{k(n-1)}},$$

which, when $m \ll n$, is approximately $\approx 1 - \frac{1}{k}$. Therefore, as $n \rightarrow \infty$ the probability of missing the first measurement ℓ times in a row converges to $\left(1 - \frac{1}{k}\right)^m$. With $m = 2k$,

$$\lim_{k \rightarrow \infty} \left(1 - \frac{1}{k}\right)^{2k} = \exp(-2),$$

and for any $k \geq 4$, $\left(1 - \frac{1}{k}\right)^{2k} \geq 0.1$ (note that this limit is to be taken only after taking $n \rightarrow \infty$). So even for arbitrarily large values of m and k , so long as $m \ll n$, there is a fixed positive probability that the RIP fails to be satisfied for the optimized without-replacement sampling scheme.

On the other hand, optimized Bernoulli selector sampling will have the RIP with vanishing probability of failure as m gets larger. Indeed, for $m \geq k$, the optimized probability weights are $\mathbf{w}^* = \left\{1, \frac{m-1}{n-1}, \dots, \frac{m-1}{n-1}\right\}$, whereby the first measurement is always sampled. There is still a positive probability that the RIP will not be satisfied due to the total number of sampled measurements \tilde{m} potentially falling below the required k . The probability of this event vanishes for $m = 2k$ as $k \rightarrow \infty$ because \tilde{m} concentrates around m with sub-Gaussian norm of order \sqrt{m} (see, e.g., [Rudelson and Vershynin(2008)]).

7 Numerics

We performed a range of experiments measuring the performance of the optimized Bernoulli sampling scheme in signal recovery problems, recovering images from the CELEBA dataset [Liu et al.(2015)Liu, Luo, Wang, and Tang], which are of size $128 \times 112 \times 3$, with total dimension $n = 43008$. For the unitary part of the CS matrix F we use the two-dimensional DFT, applied channel-wise on the three color channels of the images. We run every experiment on two different prior sets: sparse signals in the Haar wavelet basis with three levels, and signals generated by a feedforward neural network. We briefly describe how we compute an (approximate) local coherence vector, and then (approximately) solve the recovery optimization problem of Equation (2.1) in each setting.

7.1 Sparsity-based prior

We consider images from the CELEBA dataset that are truncated to their largest 500 coefficients (1%) in the Haar wavelet basis of three levels. The coherence vector α is computed with respect to the Haar basis vectors. While this does not exactly match the assumptions of our theory—which require coherence relative to the set of k -sparse vectors rather than 1-sparse vectors—it serves as a tractable heuristic consistent with standard notions of local coherence in sparse signal recovery. For the Haar basis Φ , a measurement vector \mathbf{f}_i has a local coherence $\max_{\phi \in \Phi} |\mathbf{f}_i^* \phi|$. The computation is sped up significantly by considering a representative subset of the Haar basis vectors, including one Haar wavelet basis vector for each block of Haar wavelets, utilizing the fact that translations of the support of wavelet vectors does not affect their local coherences in the Fourier basis. This method contrasts with that of [Krahmer and Ward(2014)], where they derive an upper-bound on the local coherences.

To recover the signal, we utilize basis pursuit denoising with the SPGL1 solver. From the solution, we take as support the indices supporting the most mass. Restricting to this support, we then solve a least-squares problem, which yields our recovered signal $\hat{\mathbf{x}}$.

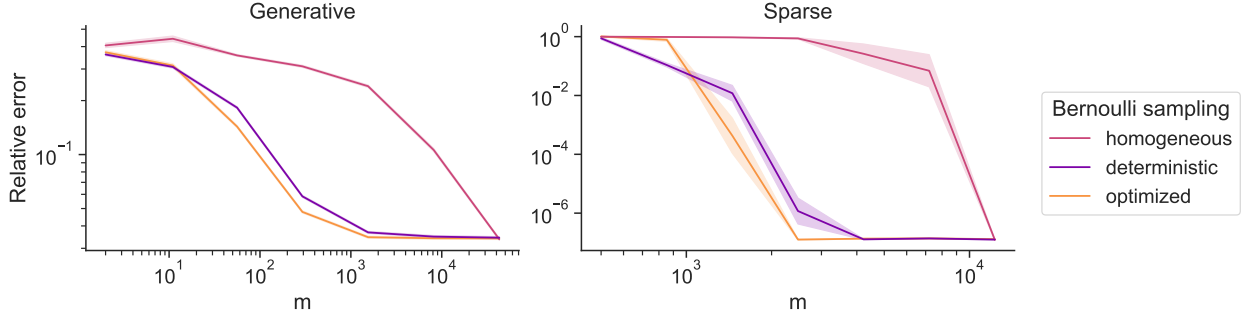


Figure 2: The generative plot has 200 experiments for each data point, and the sparse plot has 20. Sparsity level is $k = 500$ (1%) and the code dimension of the generative model is $k = 200$ (0.5%). We display a line for geometric mean and a band for the geometric standard error (the uncertainty of the geometric mean estimator).

7.2 Generative prior

We train a convolutional VAE on the CELEBA dataset, using the decoder part of the VAE as our feedforward neural network $G : \mathbb{R}^k \rightarrow \mathbb{R}^n$ with $k = 200$ (0.5%). We compute the coherence vector with respect to a random sample in the range of G , in the manner described in [Cardenas et al.(2023)Cardenas, Adcock, and Dexter, Berk et al.(2023)Berk, Brugiapaglia, Plan, Scott, Sheng, and Yilmaz]. We then attempt to recover a randomly sampled true signal $\mathbf{x}_0 = G(\mathbf{z})$ for $\mathbf{z} \sim \mathcal{N}(0, I_k)$. We sample S , compute the measurements $\mathbf{b} = SF\mathbf{x}_0$, and solve the optimization problem

$$\underset{\mathbf{z} \in \mathbb{R}^k}{\text{minimize}} \|\tilde{D}SFG(\mathbf{z}) - \tilde{D}\mathbf{b}\|_2^2.$$

To solve this program we use the LBFGS [Liu and Nocedal(1989)] algorithm with 4 steps, running 5 attempts with random restarts, and using the result of the attempt with the smallest objective value. We find an approximate minimizer $\hat{\mathbf{z}} \in \mathbb{R}^k$, and a recovered signal $\hat{\mathbf{x}} := G(\hat{\mathbf{z}})$.

7.3 Experiments

In all experiments, we use an adjusted version of Bernoulli selector sampling: with the optimized Bernoulli probability weights, we resample S until exactly m measurement vectors are selected. This is numerically trivial, and is justified by the fact that the costly operation in the compressed sensing model is not in sampling the measurement vectors, but in actually measuring the true signal (computing $\mathbf{b} := SF\mathbf{x}_0$). The sampling distribution in our experiments is therefore optimized Bernoulli selectors conditioned on the total number of sampled measurement vectors matching the expected number of sampled measurements m . In all experiments we compute the relative error $\|\hat{\mathbf{x}} - \mathbf{x}_0\|_2 / \|\mathbf{x}_0\|_2$.

Optimized sampling is a compromise between two canonical approaches: using the set of measurement vectors with the highest coherence, and using a uniformly random subset of the measurement vectors which diversifies between all possible measurement vectors. Uniform randomization was the main object of study in compressed sensing. In Figure 2 we see that when comparing optimized sampling with alternatives, optimized sampling generally performs the best. We note that for very sparse signals ($k < 200$), we found that deterministic sampling outperforms optimized sampling.

In Figure 3 we compare Bernoulli selector sampling to with-replacement sampling, a sampling distribution common in the literature (see, e.g., [Plan et al.(2025)Plan, Scott, Sheng, and Yilmaz]). We find that optimized Bernoulli selector sampling outperforms with-replacement sampling, which can be explained by the tendency of optimized with-replacement sampling to include the same high-coherence measurement vectors repeatedly in the CS matrix. Redundant measurement vectors do not provide any additional information about the true signal, other than in their denoising properties, so the CS matrix will effectively contain a smaller number of measurement vectors. This shortcoming was addressed in [Hoppe et al.(2023)Hoppe, Kraher, Verdun, Menzel, and Rauhut], where the authors provided theoretical guarantees for an optimized without-replacement sampling scheme, which we include in Figure 3. The preconditioner introduced in [Hoppe et al.(2023)Hoppe, Kraher, Verdun, Menzel, and Rauhut] simulates sampling vectors with-replacement until there are the desired number of distinct measurement vectors. Then, they include each distinct measurement vector only once in the CS matrix, removing the measurement cost of duplicate measurement vectors. They incorporate the count of redundant sampling for each measurement vector in the preconditioner, so that theoretical guarantees from with-replacement sampling carry over to this without-replacement sampling coun-

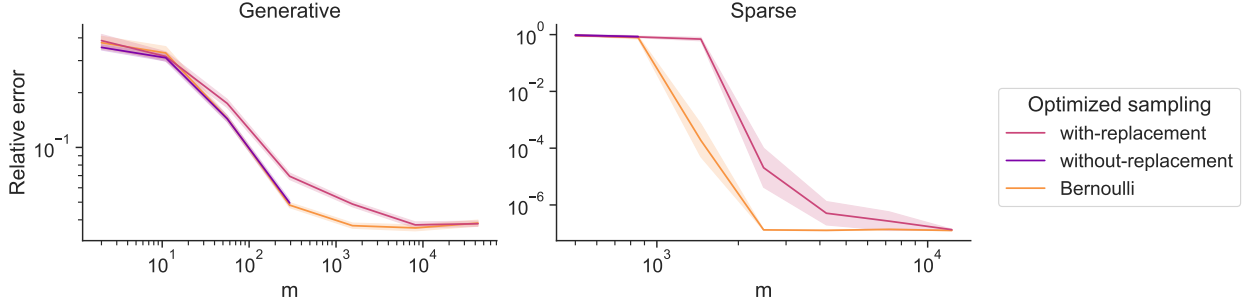


Figure 3: Comparison between optimized sampling distribution. The generative plot has 200 experiments for each data point, and the sparse plot has 20. We display a line for geometric mean and a band for the geometric standard error (the uncertainty of the geometric mean estimator). Sparsity level is $k = 500$ (1%) and the code dimension of the generative model is $k = 200$ (0.5%).

terpart. The main drawback of this method is that to compute this “empirical” preconditioner, it is necessary to use rejection sampling, with no recourse to conditional probability distributions, because the preconditioner is formulated with the count of rejections for each measurement vector.

Sampling this way proved computationally infeasible for large numbers of measurements and steeply decaying local coherences. Indeed, once the measurement vectors with high local coherence have already been sampled, the remaining unsampled measurement vectors have vanishingly small combined probability mass relative to their sampled counterparts. The number of attempts required to sample the next novel measurement vector becomes too large for even a fast loop on a computer. We stopped evaluating this method in Figure 3 when the computational cost grew too large, even with reasonably optimized code (whenever the estimated number of sampling attempts reached 10^7).

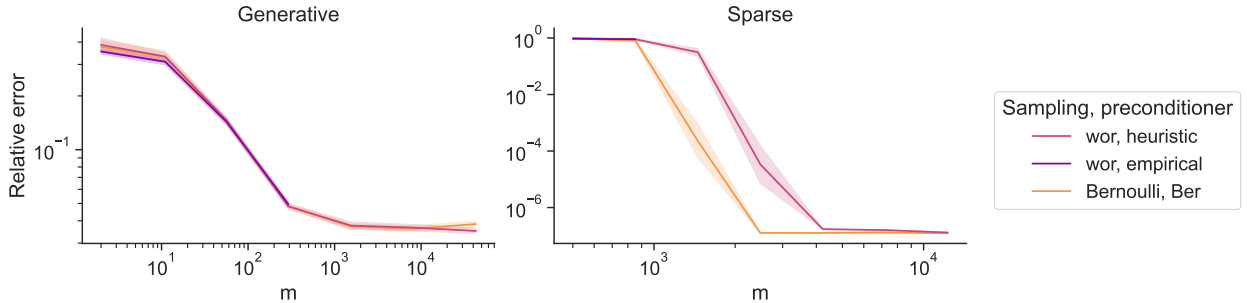


Figure 4: Comparison of optimized without-replacement sampling with two different preconditioners with the optimized Bernoulli sampling scheme. The label “wor” denotes optimized without-replacement sampling, with “empirical” preconditioning as in [Hoppe et al.(2023)Hoppe, Kraemer, Verdun, Menzel, and Rauhut], and “heuristic” preconditioning as introduced in the text. The label “Bernoulli, Ber” denotes the optimized Bernoulli sampling scheme with the Bernoulli preconditioner. The generative plot has 200 experiments for each data point, and the sparse plot has 20. We display a line for geometric mean and a band for the geometric standard error (the uncertainty of the geometric mean estimator). Note that in the Generative plot, the Bernoulli curve on the left plot is mostly underneath the “wor, heuristic” curve. Sparsity level is $k = 500$ (1%) and the code dimension of the generative model is $k = 200$ (0.5%).

In Figure 4, we sidestep the computational difficulties of without-replacement sampling with the empirical preconditioner of [Hoppe et al.(2023)Hoppe, Kraemer, Verdun, Menzel, and Rauhut] by using a alternative, heuristic, but easily computable preconditioner D , which we now describe. Given that we are sampling without-replacement with probabilities \mathbf{p} with $\sum_{i=1}^n p_i = 1$, we use a heuristic for the marginal sampling probabilities of measurement vectors to be $w_i = 1 - \exp(-\lambda p_i)$ for some constant $\lambda > 0$ chosen so that $\sum_{i=1}^n w_i = m$. We then use the preconditioner D with diagonal entries $d_i = \sqrt{\frac{m}{nw_i}}$. Though this preconditioner lacks theoretical guarantees, in Figure 4 it performs slightly better than the preconditioner from [Hoppe et al.(2023)Hoppe, Kraemer, Verdun, Menzel, and Rauhut], in the regime where the empirical preconditioner can be efficiently computed.

One important numerical result we find is that in Figure 4, the optimized Bernoulli sampling scheme outperforms the optimized without-replacement sampling scheme in the sparse setting. We believe this occurs because the local coherences have a heavier tail in the sparse setting than in the generative setting. A heavy tail provides the potential of “distracting” the optimized without-replacement sampling scheme away from the most important measurement vectors, whereas optimized Bernoulli is immune to this kind of distraction because of its ability to sample the important measurement vectors deterministically, as exemplified in the toy problem of Section 6.

We note that in other experiments not presented in this paper, we found similar performance when using the preconditioner from the optimized Bernoulli sampling scheme paired with the optimized without-replacement sampling scheme, as when using the heuristic preconditioner introduced above. Additionally, in a preliminary investigation we found that it is possible to achieve moderate performance gains by regularizing the preconditioner with a small additive constant in the denominator ($d_i = \sqrt{\frac{m}{n(w_i + 10^{-7}m)}}$). We do not use this constant in the experiments presented herein for closer correspondence to our theory.

8 Proofs

8.1 RIP of preconditioned subsampled unitary matrices

We begin with the case where the prior set is a single subspace.

Lemma 8.1 (Deviation of Bernoulli matrix on subspace). *Let $F \in \mathbb{K}^{n \times n}$ be a unitary matrix, $S \in \mathbb{R}^{m \times n}$ a Bernoulli selector sampling matrix with probability weights $\mathbf{w} \in (0, 1]^n \cap m\Delta^{n-1}$. Let $\boldsymbol{\alpha} \in \mathbb{R}_{++}^n$ be the local coherences of F with respect to a ℓ -dimensional subspace $\mathcal{U} \subseteq \mathbb{R}^n$. Let $D \in \mathbb{R}^n$ be a diagonal pre-conditioning matrix with diagonal entries $D_{i,i} = \sqrt{\frac{m}{nw_i}}$. Let γ be as defined in Theorem 4.1. Let $t > 0$. Then*

$$\sup_{\mathbf{x} \in \mathcal{U} \cap \mathbb{S}^{n-1}} \left| \|SDF\mathbf{x}\|_2 - 1 \right| \lesssim \frac{\gamma(\boldsymbol{\alpha}, \mathbf{w})}{\sqrt{m}} \sqrt{\log \ell} + \frac{\gamma(\boldsymbol{\alpha}, \mathbf{w})}{\sqrt{m}} t$$

with probability at least $1 - 2 \exp(-t^2)$.

Proof of Theorem 8.1. For some $\mathbf{w} \in (0, 1]^n \cap \Delta^{n-1}$, let $\xi_i \sim \text{Ber}(w_i)$, for $i \in [n]$, be independently distributed random variables. With a slight abuse of notation, let $S \in \{0, 1\}^{m \times n}$ be a square diagonal matrix with entries $S_{i,i} = \sqrt{\frac{n}{m}} \xi_i$. This definition differs from the Bernoulli sampling matrix of Theorem 2.2 only in the fact that we do not drop the rows that take on a value of 0. Consider that this modification does not affect the truthfulness of Theorem 8.1 because the quantity $\|SDF\mathbf{x}\|_2$ remains unchanged.

In what follows, we will use the fact that $\forall \mathbf{x} \in \mathcal{U}$, $SDF\mathbf{x} = SDFP_{\mathcal{U}}^*P_{\mathcal{U}}\mathbf{x}$ where $P_{\mathcal{U}}^* \in \mathbb{R}^{n \times \ell}$ is a matrix whose columns make an orthonormal basis for \mathcal{U} . Notice that $P_{\mathcal{U}}^*P_{\mathcal{U}} = \Pi_{\mathcal{U}} \in \mathbb{R}^{n \times n}$, the orthogonal projection on to \mathcal{U} . Now consider

$$(\star) := \sup_{\mathbf{x} \in \mathcal{U} \cap \mathbb{S}^{n-1}} \left| \|SDF\mathbf{x}\|_2^2 - 1 \right| = \sup_{\mathbf{x} \in \mathcal{U} \cap \mathbb{S}^{n-1}} \left| \|SDFP_{\mathcal{U}}^*P_{\mathcal{U}}\mathbf{x}\|_2^2 - 1 \right| \quad (8.1)$$

$$= \sup_{\mathbf{u} \in \mathbb{R}^{\ell} \cap \mathbb{S}^{\ell-1}} \left| \|SDFP_{\mathcal{U}}^*\mathbf{u}\|_2^2 - 1 \right| \quad (8.2)$$

$$= \sup_{\mathbf{u} \in \mathbb{R}^{\ell} \cap \mathbb{S}^{\ell-1}} \left| \mathbf{u}^* [P_{\mathcal{U}}F^*DS^*SDFP_{\mathcal{U}}^* - I] \mathbf{u} \right|. \quad (8.3)$$

Equation (8.2) follows from a change of variables $P_{\mathcal{U}}\mathbf{x} = \mathbf{u} \in \mathbb{R}^{\ell}$. The matrix in the square brackets is Hermitian, and therefore, $\mathbf{u}^*[\dots]\mathbf{u}$ is a real number (see, e.g., by [Axler(2024), Result 7.15]). We can therefore take the real part of the Hermitian matrix:

$$= \sup_{\mathbf{u} \in \mathbb{R}^{\ell} \cap \mathbb{S}^{\ell-1}} \left| \mathbf{u}^* \mathcal{R} [P_{\mathcal{U}}F^*DS^*SDFP_{\mathcal{U}}^* - I] \mathbf{u} \right| \quad (8.4)$$

$$= \sup_{\mathbf{u} \in \mathbb{R}^{\ell} \cap \mathbb{S}^{\ell-1}} \left| \mathbf{u}^* \mathcal{R} \left[\sum_{i=1}^n \left(\frac{1}{w_i} \xi_i - 1 \right) P_{\mathcal{U}}F^* \mathbf{e}_i \mathbf{e}_i^* F P_{\mathcal{U}}^* \right] \mathbf{u} \right| \quad (8.5)$$

$$= \left\| \sum_{i=1}^n \left(\frac{\xi_i}{w_i} - 1 \right) \mathcal{R} [P_{\mathcal{U}}F^* \mathbf{e}_i \mathbf{e}_i^* F P_{\mathcal{U}}^*] \right\|. \quad (8.6)$$

$$(8.7)$$

Notice that we have a sum of independent random matrices. As the central ingredient of this proof, we make use of the Matrix Bernstein inequality to bound Equation (8.6).

Lemma 8.2 (Matrix Bernstein). *Let X_1, \dots, X_N be independent, mean zero, symmetric random matrices in $\mathbb{R}^{\ell \times \ell}$, such that $\|X_i\| \leq K$ almost surely for all $i \in [N]$. Then, for every $t \geq 0$, we have*

$$\mathbb{P} \left\{ \left\| \sum_{i=1}^N X_i \right\| \geq t \right\} \leq 2\ell \exp \left(-\frac{t^2/2}{\sigma^2 + Kt/3} \right),$$

where $\sigma^2 = \|\sum_{i=1}^N \mathbb{E} X_i^2\|$.

We first find K . For any $i \in [n]$,

$$\begin{aligned} & \left\| \left(\frac{1}{w_i} \xi_i - 1 \right) \mathcal{R}[P_{\mathcal{U}} F^* \mathbf{e}_i \mathbf{e}_i^* F P_{\mathcal{U}}] \right\| \\ & \leq \max \left(\frac{1 - w_i}{w_i}, 1 \right) \mathbf{1}_{\{w_i < 1\}} \sup_{\mathbf{u} \in \mathbb{R}^{\ell} \cap \mathbb{S}^{\ell-1}} |\mathbf{u}^* \mathcal{R}[P_{\mathcal{U}} F^* \mathbf{e}_i \mathbf{e}_i^* F P_{\mathcal{U}}] \mathbf{u}| \\ & = \sup_{\mathbf{u} \in \mathbb{R}^{\ell} \cap \mathbb{S}^{\ell-1}} |\mathcal{R}[\|\mathbf{e}_i^* F P_{\mathcal{U}} \mathbf{u}\|_2^2]| \max \left(\frac{1 - w_i}{w_i}, 1 \right) \mathbf{1}_{\{w_i < 1\}} \\ & = \alpha_i^2 \max \left(\frac{1 - w_i}{w_i}, 1 \right) \mathbf{1}_{\{w_i < 1\}} \\ & \leq \frac{\gamma^2(\boldsymbol{\alpha}, \mathbf{w})}{m} \end{aligned}$$

Now for σ^2 , with $\mathbf{v}_i = P_{\mathcal{U}} F^* \mathbf{e}_i$,

$$\sigma^2 = \left\| \sum_{i=1}^n \mathbb{E} \left[\left(\frac{\xi_i}{w_i} - 1 \right)^2 \mathcal{R}(\mathbf{v}_i \mathbf{v}_i^*)^2 \right] \right\| \quad (8.8)$$

$$\leq \sum_{i=1}^n \max \left(\frac{1 - w_i}{w_i}, 1 \right) \mathbf{1}_{\{w_i < 1\}} \|\mathcal{R}(\mathbf{v}_i \mathbf{v}_i^*)\|^2. \quad (8.9)$$

To bound $\|\mathcal{R}(\mathbf{v}_i \mathbf{v}_i^*)\|^2$, we introduce the unit vector $\hat{\mathbf{y}}$ to be the normalization of $\mathbf{y} := \mathcal{R}[\mathbf{v}_i \mathbf{v}_i^*] \mathbf{x}$, and then

$$\begin{aligned} \mathbf{x}^* \mathcal{R}[\mathbf{v}_i \mathbf{v}_i^*] \mathcal{R}[\mathbf{v}_i \mathbf{v}_i^*] \mathbf{x} &= \mathbf{x}^* \mathcal{R}[\mathbf{v}_i \mathbf{v}_i^*] \hat{\mathbf{y}} \hat{\mathbf{y}}^* \mathcal{R}[\mathbf{v}_i \mathbf{v}_i^*] \mathbf{x} \\ &= \mathcal{R}[\mathbf{x}^* \mathbf{v}_i \mathbf{v}_i^* \hat{\mathbf{y}}] \mathcal{R}[\hat{\mathbf{y}}^* \mathbf{v}_i \mathbf{v}_i^* \mathbf{x}] \\ &\leq |\mathbf{x}^* \mathbf{v}_i|^2 |\mathbf{v}_i^* \hat{\mathbf{y}}|^2 \leq (\mathbf{x}^* \mathbf{v}_i \mathbf{v}_i^* \mathbf{x}) \alpha_i^2. \end{aligned}$$

With this,

$$\sigma^2 \leq \sum_{i=1}^n (\mathbf{x}^* \mathbf{v}_i \mathbf{v}_i^* \mathbf{x}) \max_{j \in [n]} \alpha_j^2 \max \left(\frac{1 - w_j}{w_j}, 1 \right) \mathbf{1}_{\{w_j < 1\}} = \frac{\gamma^2(\boldsymbol{\alpha}, \mathbf{w})}{m},$$

because $\sum_{i=1}^n \mathbf{v}_i \mathbf{v}_i^* = I$. Then applying Matrix Bernstein yields

$$\mathbb{P} \left\{ \sup_{\mathbf{x} \in \mathcal{U} \cap \mathbb{S}^{n-1}} \left| \|\mathcal{SDF} \mathbf{x}\|_2^2 - 1 \right| \geq t \right\} \leq 2\ell \exp \left(-\frac{m}{\gamma^2} \min(t^2, t) \right).$$

The result then follows from algebraic manipulations of this tail inequality (for the details, see, e.g., the proof of [Plan et al.(2025)Plan, Scott, Sheng, and Yilmaz, Lemma A.1]). \square

Proof of Theorem 4.2. Perform a union bound on Theorem 8.1 applied to each subspace \mathcal{U} making up \mathcal{T} . Additional details on this union bound can be found in the proof of [Plan et al.(2025)Plan, Scott, Sheng, and Yilmaz, Lemma A.1], which is similar. \square

8.2 Bounding the noise complexity

Proof of Theorem 5.3. We combine two upper-bounds.

First upper-bound

It is that of Equation (3.1) in Theorem 3.5;

$$\|\tilde{D}\mathbb{T}(SD\boldsymbol{\alpha})\|_2^2 \leq \max(\mathbf{d})^2 = L\sqrt{\frac{1}{n \min(\boldsymbol{\alpha})}}.$$

Second upper-bound

With $U = \{i \in [n] : w_i^\circ < 1\}$,

$$\|\tilde{D}\mathbb{T}(SD\boldsymbol{\alpha})\|_2^2 = \|\tilde{D}|_U\mathbb{T}(SD\boldsymbol{\alpha})|_U\|_2^2 + \|\tilde{D}|_{U^c}\mathbb{T}(SD\boldsymbol{\alpha})|_{U^c}\|_2^2.$$

We treat the two terms differently.

Term with unsaturated entries

Let $\bar{\mathbf{w}} \in \mathbb{R}_{++}^n$ be with entries $\bar{w}_i = \frac{m\alpha_i^2}{L^2}$, which is such that $\bar{\mathbf{w}} \geq \mathbf{w}^\circ$ entry-wise. Let \mathbf{h} be similar to \mathbf{d} , only that it depends on $\bar{\mathbf{w}}$ instead of \mathbf{w}° , i.e., $h_i := \sqrt{\frac{m}{n\bar{w}_i}}$, $H := \text{Diag}(\mathbf{h})$, and $\tilde{H} := \text{Diag}(\sqrt{\frac{m}{n}}S\mathbf{h})$. Then $\|\tilde{H}\mathbb{T}(SH\boldsymbol{\alpha})\|_2^2 \leq \|\tilde{D}|_U\mathbb{T}(SD\boldsymbol{\alpha})|_U\|_2^2$. So,

$$(\star) := \|\tilde{H}\mathbb{T}(SH\boldsymbol{\alpha})\|_2^2 \leq \|SH^2\boldsymbol{\alpha}\|_2^2.$$

Because $h_i = \sqrt{\frac{m}{nw_i^\circ}} = \frac{L}{\sqrt{n\alpha_i}}$, and so $H^2\boldsymbol{\alpha} = \frac{L}{\sqrt{n}}\mathbf{h}$, we get the upper-bound

$$(\star) \leq \frac{L^2}{n}\|S\mathbf{h}\|_2^2.$$

Then by Markov's inequality,

$$\mathbb{E}\|S\mathbf{h}\|_2^2 = \frac{n}{m} \sum_{i=1}^n w_i^\circ h_i^2 = \frac{m}{n} \sum_{i=1}^n w_i^\circ \frac{m}{nw_i^\circ} = n.$$

This gives us that with probability at least $1 - \delta$,

$$(\star) \leq \frac{L^2}{\delta}.$$

Saturated term

Now for the saturated terms, with \mathbf{d} , D , \tilde{D} back to being defined with \mathbf{w}° , notice that $\tilde{D} = \sqrt{\frac{m}{n}}I$, and that $\mathbb{T}(SD\boldsymbol{\alpha})$ are convex coefficients, so that

$$\|\tilde{D}|_{U^c}\mathbb{T}(SD\boldsymbol{\alpha})|_{U^c}\|_2^2 \leq \frac{m}{n}$$

Combining these upper-bounds, result follows. \square

8.3 Union bounds

Proof of Theorem 4.3. Let $t_1 > 0$, and

$$m \gtrsim \gamma^2(\boldsymbol{\alpha}, \mathbf{w})(\log(\ell) + \log M + t_1^2).$$

Then each of the following statements holds individually with probability at least $1 - 2\exp(-t^2)$ for a variable $t > 0$ defined within each of the results.

1. The matrix SDF has the RIP on \mathcal{T} thanks to Theorem 4.2.
2. When I . is satisfied, the recovery error is bounded as specified by Theorem 3.4.

We distinguish between the variables t used within each of the two statements by re-labelling them t_1, t_2 respectively. For some $\delta > 0$, let $2 \exp(-t_1^2) = \frac{1}{2}\delta$ and $2 \exp(-t_2^2) = \frac{1}{2}\delta$. Then $t_1 = t_2 = \sqrt{\log \frac{4}{\delta}}$. The fact that the second statement is conditional on the success of the first only lessens the true probability of failure, and so the probability of failure is no more than $\frac{1}{2}\delta + \frac{1}{2}\delta = \delta$. The result follows. \square

Proof of Theorem 2.8. The proof is a minor variation on the proof of Theorem 4.3.

Let $t_1 > 0$, and let

$$m \gtrsim L(\boldsymbol{\alpha}, m)^2 (\log \ell + \log M + t_1^2).$$

Each of the following statements holds individually with probability at least $1 - 2 \exp(-t^2)$ for a variable $t > 0$ defined within each of the three results.

1. The matrix SDF has the RIP thanks to Theorem 4.2, by bounding γ by η and evaluating at the optimized probability weights \boldsymbol{w}° .
2. When 1. is satisfied, the recovery error is bounded as specified by Theorem 3.4.
3. When 1. is satisfied, the noise sensitivity $\|\tilde{D}\mathbb{T}(SD\boldsymbol{\alpha})\|_2$ in the recovery error bound of Theorem 3.4 is bounded thanks to Theorem 5.3.

We distinguish between the variables t used within each of the three statements by re-labelling them t_1, t_2, t_3 respectively. For some $\delta > 0$, let $2 \exp(-t_1^2) = \frac{1}{10}\delta$, $2 \exp(-t_2^2) = \frac{1}{10}\delta$, and $t_3 = \frac{8}{10}\delta$. Then $t_1 = t_2 = \sqrt{\log \frac{20}{\delta}}$. The required statement then holds with probability at least $1 - \delta$ from a union bound on the three statements above for this choice of t_1, t_2, t_3 . \square

8.4 Optimizing the sampling scheme

We begin with a lemma for a larger class of optimization problems.

Lemma 8.3 (On the element wise maximized objectives with soft boundaries). *Take a number of decreasing functions f_1, \dots, f_n , which are of the form $f_i : (0, 1] \rightarrow \mathbb{R} \forall i \in [n]$. For $\beta > 0$, consider the optimization problem*

$$\text{minimize } \max_{j \in [n]} f_j(w_j) \text{ s.t. } \boldsymbol{w} \in \beta \Delta^{n-1}.$$

We have that:

1. Any point $\boldsymbol{w}^* \in \beta \Delta^{n-1}$ such that

$$\forall i \in [n], \quad \lim_{w_i \uparrow w_i^*} f_i(w_i) \geq \max_{j \in [n]} f_j(w_j^*) \tag{8.10}$$

is a minimizer. Here, “ \uparrow ” denotes a left limit.

2. If the functions f_1, \dots, f_n are moreover strictly decreasing, then the minimizer \boldsymbol{w}^* in (1.) is unique.

Proof of Theorem 8.3. Let $\boldsymbol{w}^* \in \beta \Delta^{n-1}$ satisfy Equation (8.10). We argue that it is impossible to find another point $\hat{\boldsymbol{w}} \neq \boldsymbol{w}^*$ in $\beta \Delta^{n-1}$ such that

$$\max_{j \in [n]} f_j(\hat{w}_j) < \max_{j \in [n]} f_j(w_j^*). \tag{8.11}$$

Since $\hat{\boldsymbol{w}} \neq \boldsymbol{w}^*$, and since they both lie in $\beta \Delta^{n-1}$, there is an $i \in [n]$ such that $\hat{w}_i < w_i^*$. Then

$$f_i(\hat{w}_i) \geq \lim_{w_i \uparrow w_i^*} f_i(w_i) \geq \max_{j \in [n]} f_j(w_j^*), \tag{8.12}$$

where the second inequality follows from Equation (8.10). But this yields a contradiction with Equation (8.11), so \boldsymbol{w}^* must be a minimizer.

The second part of the result follows from noting that when the functions are strictly decreasing, the first inequality in Equation (8.12) is strict. \square

With Theorem 8.3 we prove the results of Section 8.4.

Proof of Theorem 5.2. We use Theorem 8.3 with the functions $f_i(x) := \alpha_i \sqrt{\frac{m}{x}} \mathbf{1}_{\{x < 1\}}$, which are strictly decreasing for all $i \in [n]$, and which satisfy $\max_{i \in [n]} f_i(w_i^\circ) = \eta(\boldsymbol{\alpha}, \mathbf{w}^\circ)$. Since $\eta(\boldsymbol{\alpha}, \mathbf{w}^\circ) = L$, it remains only to show that $\forall i \in [n], \lim_{w_i \uparrow w_i^\circ} f_i(w_i) \geq L$.

For any fixed *unsaturated* entry $i \in [n]$, f_i is continuous in a neighborhood of w_i° , so it is sufficient to show that $f_i(w_i^\circ) \geq L$. This holds because with the formula $w_i^\circ = \frac{m\alpha_i^2}{L^2}$, one can compute that $f_i(w_i^\circ) = L$.

Second, for any *saturated* entry $i \in [n]$, we know from the definition of \mathbf{w}° that $\frac{\alpha_i^2 m}{L^2(\boldsymbol{\alpha}, m)} \geq 1$, and therefore,

$$\lim_{w_i \uparrow 1} f_i(w_i) = \lim_{w_i \uparrow 1} \alpha_i \sqrt{\frac{m}{w_i}} = \alpha_i \sqrt{m} \geq L.$$

□

8.5 Properties of the optimized sampling scheme

Proof of Theorem 2.7. WLOG let $\boldsymbol{\alpha}$ be increasing (otherwise, re-index it). Note that J is well-defined because the set over which we take a maximum is non-empty. Indeed,

$$\frac{m\alpha_1^2}{R^2(1; \boldsymbol{\alpha}, m)} = 1 - (n - m) < 1,$$

because $m < n$.

We show that the index J identifies the last unsaturated entry of the optimized weights. The entry J is unsaturated because

$$w_J^\circ = \frac{m\alpha_J^2}{L^2(\boldsymbol{\alpha}, m)} = \frac{m\alpha_J^2}{R^2(J; \boldsymbol{\alpha}, m)} < 1$$

by definition of J . If $J = n$, J is indeed the last unsaturated entry. If $J < n$, then the entry $J + 1$ satisfies

$$\begin{aligned} & \frac{m\alpha_{J+1}^2}{R^2(J+1; \boldsymbol{\alpha}, m)} \geq 1 \\ \implies & \frac{\alpha_{J+1}^2}{\left(\frac{\|\boldsymbol{\alpha}_{|\leq J+1}\|_2^2}{m - (n - (J+1))}\right)} \geq 1 \\ \implies & \alpha_{J+1}^2 (J - (n - m) + 1) \geq \|\boldsymbol{\alpha}_{|\leq J+1}\|_2^2 \\ \implies & \alpha_{J+1}^2 (J - (n - m)) \geq \|\boldsymbol{\alpha}_{|\leq J}\|_2^2 \\ \implies & \frac{\alpha_{J+1}^2}{\left(\frac{\|\boldsymbol{\alpha}_{|\leq J}\|_2^2}{(J - (n - m))}\right)} \geq 1 \\ \implies & \frac{m\alpha_{J+1}^2}{L^2(\boldsymbol{\alpha}, m)} \geq 1. \end{aligned}$$

and so $w_{J+1}^\circ = 1$. Since the expression $\frac{m\alpha_j^2}{L^2(\boldsymbol{\alpha}, m)}$ is monotone in j , this means that $w_j^\circ = 1$ for $j > J$ and $w_j^\circ < 1$ for $j \leq J$.

Then

$$\begin{aligned} \sum_{j=1}^n w_j^\circ &= \sum_{j=1}^J \frac{m\alpha_j^2}{L^2(\boldsymbol{\alpha}, m)} + \sum_{j=J+1}^n 1 \\ &= \frac{m(J - (n - m))}{m\|\boldsymbol{\alpha}_{|[J]}\|_2^2} \left(\sum_{i=1}^J \alpha_i^2 \right) + n - J \\ &= m. \end{aligned}$$

□

Proof of Theorem 2.10. We begin by showing that the upper-bound holds. Consider $f(x) := \sum_{i=1}^n \min\left(\frac{\alpha_i^2}{x}, 1\right) - m$ and $g(x) := \sum_{i=1}^n \frac{\alpha_i^2}{x} - m$. They are strictly decreasing functions and $\forall x \in \mathbb{R}, f(x) \leq g(x)$. It follows that the root of g must be greater than the root of f . By inspection, the root of f is L and the root of g is $\|\alpha\|_2$, and so the upper-bound in the statement follows.

For the lower bound, first we recall the definition of the variable J in Theorem 5.2 to be $J := \max\left\{J \in [n] : \frac{\|\alpha_{\leq J}\|_2^2}{\alpha_J^2} > (m - (n - J) - 1)\right\}$. Then we see that $J \geq n - m + 1$ since if we let $J = n - m + 1$, the r.h.s. in the inequality in the definition of J is zero, and the l.h.s. is always strictly positive since we assumed strictly positive local coherences. Then the lower-bound holds because

$$L^2 := \|\alpha_{\leq J}\|_2^2 \frac{m}{(m - (n - J))} \geq \|\alpha_{\leq J}\|_2^2 \geq \|\alpha_{\leq n-m+1}\|_2^2.$$

□

Proof of Theorem 2.11. For some fixed $m \in \mathbb{N}$ and local coherences $\alpha \in \mathbb{R}_{++}^n$, the optimized probability w^* from Theorem 5.2 is contained in $m\Delta^{n-1}$. Therefore,

$$\sum_{i=1}^n w_i^* = \sum_{i=1}^n \min\left(\frac{m\alpha_j^2}{L^2(m)}, 1\right) = m,$$

where denote L as a function of m . We solve for its first derivative $L'(m)$ by implicit differentiation. Differentiating by m and isolating $L'(m)$, we find that

$$\text{sgn}(L') = \text{sgn}\left(1 - \frac{L^2}{\|\alpha_{\leq J}\|_2^2}\right).$$

That $L \geq \|\alpha_{\leq J}\|_2$ follows from the proof of Theorem 2.10. □

Acknowledgements

Large language models were used while writing the manuscript for help with grammar and phrasing (Claude, Grok, and Chatgpt).

Funding

Y. Plan is partially supported by an NSERC Discovery Grant (GR009284), an NSERC Discovery Accelerator Supplement (GR007657), and a Tier II Canada Research Chair in Data Science (GR009243). O. Yilmaz was supported by an NSERC Discovery Grant (22R82411). O. Yilmaz also acknowledges support by the Pacific Institute for the Mathematical Sciences (PIMS) and the CNRS – PIMS International Research Laboratory.

Data availability

The data underlying the numerical experiments in this article are available in the CELEBA dataset [Liu et al.(2015)Liu, Luo, Wang, and Tang] and the flower dataset [Nilsback and Zisserman(2008)]. No new datasets were generated for this study.

References

- [Adcock et al.(2024)Adcock, Cardenas, and Dexter] B. Adcock, J. M. Cardenas, and N. Dexter. A Unified Framework for Learning with Nonlinear Model Classes from Arbitrary Linear Samples. In *Proceedings of the 41st International Conference on Machine Learning*, pages 169–202. PMLR, July 2024.
- [Axler(2024)] S. Axler. *Linear Algebra Done Right*. Undergraduate Texts in Mathematics. Springer International Publishing, Cham, 2024. ISBN 978-3-031-41025-3 978-3-031-41026-0. doi: 10.1007/978-3-031-41026-0.
- [Berk et al.(2022)Berk, Brugiapaglia, Joshi, Plan, Scott, and Yilmaz] A. Berk, S. Brugiapaglia, B. Joshi, Y. Plan, M. Scott, and Ö. Yilmaz. A Coherence Parameter Characterizing Generative Compressed Sensing With Fourier Measurements. *IEEE Journal on Selected Areas in Information Theory*, 3(3):502–512, Sept. 2022. ISSN 2641-8770. doi: 10.1109/JSAIT.2022.3220196.

- [Berk et al.(2023)Berk, Brugiapaglia, Plan, Scott, Sheng, and Yilmaz] A. Berk, S. Brugiapaglia, Y. Plan, M. Scott, X. Sheng, and O. Yilmaz. Model-adapted Fourier sampling for generative compressed sensing. In *NeurIPS 2023 Workshop on Deep Learning and Inverse Problems*, Nov. 2023.
- [Bigot et al.(2016)Bigot, Boyer, and Weiss] J. Bigot, C. Boyer, and P. Weiss. An Analysis of Block Sampling Strategies in Compressed Sensing. *IEEE Transactions on Information Theory*, 62(4):2125–2139, Apr. 2016. ISSN 1557-9654. doi: 10.1109/TIT.2016.2524628.
- [Candes and Romberg(2007)] E. Candes and J. Romberg. Sparsity and Incoherence in Compressive Sampling. *Inverse Problems*, 23(3):969–985, June 2007. ISSN 0266-5611, 1361-6420. doi: 10.1088/0266-5611/23/3/008.
- [Cardenas et al.(2023)Cardenas, Adcock, and Dexter] J. M. Cardenas, B. Adcock, and N. Dexter. CS4ML: A general framework for active learning with arbitrary data based on Christoffel functions. *Advances in Neural Information Processing Systems*, 36:19990–20037, Dec. 2023.
- [Chauffert et al.(2014)Chauffert, Ciuciu, Kahn, and Weiss] N. Chauffert, P. Ciuciu, J. Kahn, and P. Weiss. Variable Density Sampling with Continuous Trajectories. *SIAM J. Img. Sci.*, 7(4):1962–1992, Jan. 2014. doi: 10.1137/130946642.
- [Hoppe et al.(2023)Hoppe, Krahmer, Verdun, Menzel, and Rauhut] F. Hoppe, F. Krahmer, C. M. Verdun, M. I. Menzel, and H. Rauhut. Sampling Strategies for Compressive Imaging Under Statistical Noise. In *2023 International Conference on Sampling Theory and Applications (SampTA)*, 2023 International Conference on Sampling Theory and Applications, SampTA 2023. Institute of Electrical and Electronics Engineers Inc., 2023. doi: 10.1109/SampTA59647.2023.10301372.
- [Krahmer and Ward(2014)] F. Krahmer and R. Ward. Stable and Robust Sampling Strategies for Compressive Imaging. *IEEE Trans. on Image Process.*, 23(2):612–622, Feb. 2014. ISSN 1057-7149, 1941-0042. doi: 10.1109/TIP.2013.2288004.
- [Liu and Nocedal(1989)] D. C. Liu and J. Nocedal. On the limited memory BFGS method for large scale optimization. *Mathematical Programming*, 45(1):503–528, Aug. 1989. ISSN 1436-4646. doi: 10.1007/BF01589116.
- [Liu et al.(2015)Liu, Luo, Wang, and Tang] Z. Liu, P. Luo, X. Wang, and X. Tang. Deep Learning Face Attributes in the Wild. In *Proceedings of the 2015 IEEE International Conference on Computer Vision (ICCV)*, ICCV ’15, pages 3730–3738, USA, Dec. 2015. IEEE Computer Society. ISBN 978-1-4673-8391-2. doi: 10.1109/ICCV.2015.425.
- [Lustig et al.(2007)Lustig, Donoho, and Pauly] M. Lustig, D. Donoho, and J. M. Pauly. Sparse MRI: The application of compressed sensing for rapid MR imaging. *Magn Reson Med*, 58(6):1182–1195, Dec. 2007. ISSN 0740-3194. doi: 10.1002/mrm.21391.
- [Nilsback and Zisserman(2008)] M.-E. Nilsback and A. Zisserman. Automated Flower Classification over a Large Number of Classes. In *2008 Sixth Indian Conference on Computer Vision, Graphics & Image Processing*, pages 722–729, Dec. 2008. doi: 10.1109/ICVGIP.2008.47.
- [Plan et al.(2025)Plan, Scott, Sheng, and Yilmaz] Y. Plan, M. S. Scott, X. Sheng, and O. Yilmaz. Denoising guarantees for optimized sampling schemes in compressed sensing, Apr. 2025.
- [Polak et al.(2015)Polak, Duarte, and Goeckel] A. C. Polak, M. F. Duarte, and D. L. Goeckel. Performance Bounds for Grouped Incoherent Measurements in Compressive Sensing. *IEEE Trans. Signal Process.*, 63(11):2877–2887, June 2015. ISSN 1053-587X, 1941-0476. doi: 10.1109/TSP.2015.2412912.
- [Puy et al.(2011)Puy, Vandergheynst, and Wiaux] G. Puy, P. Vandergheynst, and Y. Wiaux. On Variable Density Compressive Sampling. *IEEE Signal Process. Lett.*, 18(10):595–598, Oct. 2011. ISSN 1070-9908, 1558-2361. doi: 10.1109/LSP.2011.2163712.
- [Rudelson and Vershynin(2008)] M. Rudelson and R. Vershynin. On sparse reconstruction from Fourier and Gaussian measurements. *Comm. Pure Appl. Math.*, 61(8):1025–1045, Aug. 2008. ISSN 00103640, 10970312. doi: 10.1002/cpa.20227.

A Equivalence of duplicate-rejection sampling and sequential renormalized sampling

Proposition A.1 (Equivalence of two without-replacement implementations). *Let $F = \{f_1, \dots, f_n\}$ and let $p = (p_1, \dots, p_n)$ satisfy $p_j \geq 0$ and $\sum_{j=1}^n p_j = 1$. Fix $1 \leq m \leq n$. Consider the following two procedures that generate an ordered m -tuple of distinct indices (I_1, \dots, I_m) .*

- (1) **Duplicate-rejection (with-replacement) sampling.** Draw i.i.d. random variables X_1, X_2, \dots with $\mathbb{P}(X_t = j) = p_j$. Accept a draw if it has not appeared previously among accepted values; otherwise reject it and continue. Stop after m distinct values have been accepted, and denote the accepted sequence by (I_1, \dots, I_m) .
- (2) **Sequential sampling without replacement with renormalization.** Set $S_0 = \emptyset$. For $r = 1, \dots, m$, sample I_r from $\{1, \dots, n\} \setminus S_{r-1}$ according to

$$\mathbb{P}(I_r = j \mid S_{r-1}) = \frac{p_j}{\sum_{\ell \notin S_{r-1}} p_\ell}, \quad j \notin S_{r-1},$$

and set $S_r = S_{r-1} \cup \{I_r\}$.

Then the two procedures induce the same distribution on (I_1, \dots, I_m) .

Proof. It suffices to show that, in procedure (1), conditional on the current accepted set being $S \subset \{1, \dots, n\}$, the next accepted index has the same conditional distribution as in (2).

In (1), let $q = \sum_{i \in S} p_i$. The next accepted value is the first draw outside S . For any $j \notin S$,

$$\mathbb{P}(\text{next accepted} = j) = \sum_{t=1}^{\infty} q^{t-1} p_j = \frac{p_j}{1-q} = \frac{p_j}{\sum_{\ell \notin S} p_\ell}.$$

Thus, conditional on S , the next accepted index is drawn from S^c with probabilities proportional to p_j , exactly as specified in (2).

Since the first accepted index has distribution p in both procedures and the same conditional rule governs each subsequent step, the joint law of (I_1, \dots, I_m) coincides by induction. \square

B Python code

Listing 1: Computation of the optimized Bernoulli probability weights from a local coherence vector.

```
def Optimized_Bernoulli_prob_weights(loc_co: NDArray, m: int):
    pos_co = loc_co[loc_co > 0]
    n = pos_co.size
    assert m <= n, "Cannot sample enough measurements."
    if m == n:
        samplings = np.zeros_like(loc_co)
        samplings[loc_co > 0] = 1
        return samplings, 0, 0.0
    sorted_co = np.sort(pos_co.flat)

    def Lsqrd(j, m, n, sorted_co):
        assert j > n - m - 1
        assert m <= n
        assert j <= n - 1
        return m * np.sum(sorted_co[:j + 1] ** 2) / (j - (n - m - 1))

    J = None
    for j in range(n - 1, n - m - 1, -1):
        if m * sorted_co[j] ** 2 < Lsqrd(j, m, n, sorted_co):
            J = j
            break
    if J is None:
        raise ValueError("No valid J found (should never happen).")
    Lsqr = Lsqrd(J, m, n, sorted_co)
    return np.clip(m * loc_co ** 2 / Lsqr, 0, 1), J, Lsqr
```